Bond Directional Anapole Order in a Spin-Orbit Coupled Mott Insulator $Sr_2(Ir_{1-x}Rh_x)O_4$

H. Murayama,[1] K. Ishida,[2] R. Kurihara,[1] T. Ono,[1] Y. Sato,[1] Y. Kasahara,[1] H. Watanabe,[1] Y. Yanase,[1,4] G. Cao,[3] Y. Mizukami,[2] T. Shibauchi,[2] Y. Matsuda,[1] and S. Kasahara[1]

[1]*Department of Physics, Kyoto University, Kyoto 606-8502 Japan*
[2]*Department of Advanced Materials Science, University of Tokyo, Chiba 277-8561, Japan*
[3]*Department of Physics, University of Colorado at Boulder, Boulder, Colorado 80309, USA*
[4]*Institute for Molecular Science, Okazaki 444-8585, Japan*

(Received 5 August 2020; revised 3 November 2020; accepted 4 December 2020; published 2 February 2021)

An anapole state that breaks inversion and time-reversal symmetries while preserving translation symmetry of an underlying lattice has aroused great interest as a new quantum state, but only a few candidate materials have been reported. Recently, in a spin-orbit coupled Mott insulator $Sr_2(Ir_{1-x}Rh_x)O_4$, the emergence of a possible hidden-order phase with broken inversion symmetry has been suggested at T_Ω above the Néel temperature by optical second-harmonic-generation measurements. Moreover, polarized neutron diffraction measurements revealed broken time-reversal symmetry below T_Ω, which was supported by subsequent muon spin relaxation experiments. However, the nature of this mysterious phase remains largely elusive. Here, we investigate the hidden-order phase through the combined measurements of the in-plane magnetic anisotropy with exceptionally high-precision magnetic torque and the nematic susceptibility with elastoresistance. A distinct twofold in-plane magnetic anisotropy along the [110] Ir-O-Ir bond direction sets in below about T_Ω, providing thermodynamic evidence for a nematic phase transition with broken C_4 rotational symmetry. However, in contrast to the even-parity nematic transition reported in other correlated electron systems, the nematic susceptibility exhibits no divergent behavior towards T_Ω. These results provide bulk evidence for an odd-parity order parameter with broken rotational symmetry in the hidden-order state. We discuss the hidden order in terms of an anapole state, in which the polar toroidal moment is induced by two current loops in each IrO_6 octahedron of opposite chirality. Contrary to the simplest loop-current pattern previously suggested, the present results are consistent with a pattern in which the intra-unit cell loop current flows along only one of the diagonal directions in the IrO_4 square.

DOI: 10.1103/PhysRevX.11.011021

Subject Areas: Condensed Matter Physics
Strongly Correlated Materials

I. INTRODUCTION

The search for novel types of ordered states is one of the most exciting and challenging issues of modern condensed-matter physics. In strongly correlated electron systems, charge, spin, and orbital degrees of freedom generate a rich variety of ordered states. Any of these ordered states can be characterized by their behaviors under space-inversion (parity) and time-reversal operations. Among systems with broken parity, toroidal states, in which translational symmetry of the underlying lattice is preserved, have been widely discussed [1,2]. There are two types of toroidal states—axial and polar—where time-reversal symmetry is preserved and broken, respectively [3–5]. An example of the axial toroidal states are the electric-toroidal systems with a vortexlike arrangement of electric dipoles [6–8]. The order parameter of this state is represented by the electric-toroidal dipole moment $\boldsymbol{\Omega}_A$, as illustrated in Fig. 1(a). The polar toroidal state is realized in magneto-toroidal systems with a vortexlike arrangement of spin and loop currents, as illustrated in Figs. 1(b) and 1(c), respectively. The order parameter of these polar toroidal systems is represented by the polar magnetic toroidal dipole moment $\boldsymbol{\Omega}_P$. The emergence of the polar toroidal dipole moment has aroused significant interest [9–11]. In particular, the state, in which the polar toroidal dipole is induced by persistent loop currents as illustrated in Fig. 1(c), is a new quantum state of matter, and finding it has been a longstanding quest in condensed matter physics. To distinguish two polar states, as shown in Figs. 1(b) and 1(c), we call the polar toroidal state caused by the loop currents an anapole state. The order parameter of the anapole state is represented by the anapole vector $\boldsymbol{\Omega}_P \propto \int \boldsymbol{r} \times \boldsymbol{m}(\boldsymbol{r}) d^3 r$, where $\boldsymbol{r}$ and $\boldsymbol{m}$ are the position and magnetic moment induced by orbital loop currents, respectively. For ferrotoroidal coupling in a tetragonal system, where $\boldsymbol{\Omega}_A$ or $\boldsymbol{\Omega}_P$ is aligned parallel to the *ab*

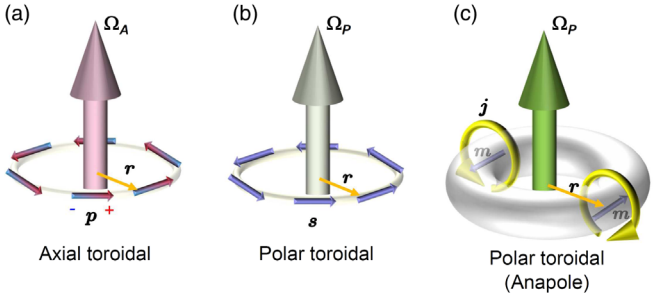

FIG. 1. Toroidal states with broken inversion symmetry. (a) Electric-toroidal state with a vortexlike arrangement of electric dipoles $\boldsymbol{p}$. This is the axial toroidal state in which time-reversal symmetry is preserved. Note that $\boldsymbol{\Omega_A} \propto \sum_i \boldsymbol{r}_i \times \boldsymbol{p}_i$ is the axial toroidal moment. (b) Magneto-toroidal state with a vortexlike arrangement of spin $\boldsymbol{s}$. This is a polar toroidal state in which time-reversal symmetry is broken. Note that $\boldsymbol{\Omega_P} \propto \sum_i \boldsymbol{r}_i \times \boldsymbol{s}_i$ is the polar toroidal moment. (c) Anapole state. The loop currents $\boldsymbol{j}$ flowing on the surface of a torus induce toroidal magnetic fields $\boldsymbol{m}$. Note that $\boldsymbol{\Omega_P} \propto \int \boldsymbol{r} \times \boldsymbol{m}(\boldsymbol{r}) d^3 r$ is the anapole vector.

plane, transnational symmetry is not broken, but spatial inversion and fourfold rotational symmetries are broken. The anapole state has been discussed in the pseudogap state in cuprates [12–21], but the presence of such a state has been highly controversial [22–24].

Recently, the layered perovskite Sr_2IrO_4 has attracted much interest because it is the first experimental realization of a spin-orbit coupled Mott insulator [25–29]. The combination of strong spin-orbit coupling and electron correlation makes this material a promising candidate that hosts a novel electronic state of matter. The crystal has a tetragonal structure of corner sharing IrO_6 octahedra, which is rotated by $\theta = 11°$ around the c axis [Figs. 2(a) and 2(b)] [30–33]. A crystalline electric field splits the energy levels of $5d^5$

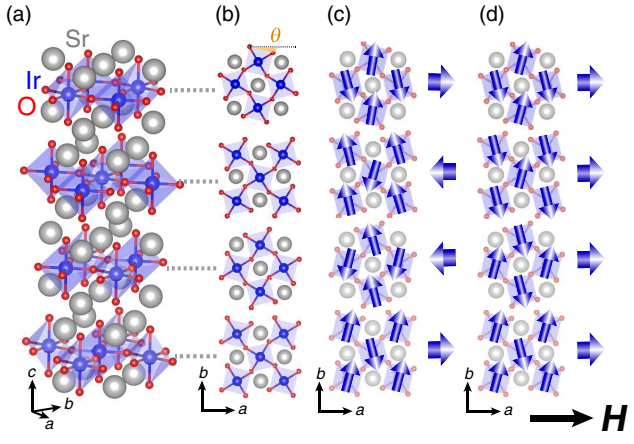

FIG. 2. (a) Crystal structure of Sr_2IrO_4. (b) Top view of each layer. The crystal has a tetragonal structure with corner sharing IrO_6 octahedra, which is rotated by $\theta = 11°$ around the c axis. (c) AF-I $(+--+)$ magnetic structure. (d) AF-II $(++++)$ magnetic structure. Weak ferromagnetic moments are induced in the plane.

electrons in the Ir^{4+} ion into e_g and t_{2g} states. The presence of a strong spin-orbit interaction splits t_{2g} states into a pseudospin $J_{\text{eff}} = 1/2$ doublet and $J_{\text{eff}} = 3/2$ quartet. A large enough Coulomb interaction splits the $J_{\text{eff}} = 1/2$ doublet, leading to a Mott insulating state with one localized electron, which is well described by the $J_{\text{eff}} = 1/2$ pseudospin anisotropic Heisenberg model [25]. Such a state has been experimentally established by angle-resolved photoemission spectroscopy (ARPES) and resonant x-ray scattering experiments [25,34]. Below $T_N \approx 240$ K, Sr_2IrO_4 exhibits a long-range antiferromagnetic (AFM) order [31,32,34]. The magnetic moments are aligned in the basal ab plane, and they follow the rotation of IrO_6 octahedra forming a canted antiferromagnetism with $(+--+)$ structure along the c axis (AF-I), as illustrated in Fig. 2(c) [34,35]. When a magnetic field of greater than or about 0.1 T is applied parallel to the ab plane, the magnetic structure of AF-I changes to that of AF-II with $(++++)$ structure as shown in Fig. 2(d), in which weak ferromagnetic moments are induced within the plane [34].

Despite the complication of the strong spin-orbit interaction, different active orbitals, and structural distortions, it has been suggested that the low-energy electronic structure of Sr_2IrO_4 bears a certain resemblance to that of the cuprates [25,36]. It has been pointed out that electron-doped iridates should be compared to hole-doped cuprates because of the opposite band curvature due to the opposite sign of the next-nearest hopping term [37]. In electron-doped Sr_2IrO_4, which is achieved by K-doping at the surface or by partial substitution of La for Sr in the bulk [38,39], ARPES and scanning tunneling microscopy measurements report the emergence of Fermi surface pockets, Fermi arcs, and d-wave-like pseudogaps [40–45], but no direct signature of the superconductivity has been reported, despite the theoretical predictions [37,46–48].

The effective hole doping is achieved by Rh substitution [49,50]. It has been shown that Rh ions act as acceptors by forming a $Rh^{3+}(4d^6)$ oxidation state, creating nearby $Ir^{5+}(5d^4)$ ions to preserve the charge neutrality [51]. The T–x phase diagram of $Sr_2(Ir_{1-x}Rh_x)O_4$ is displayed in Fig. 3. The AFM transition temperature decreases almost linearly as a function of x and vanishes at a critical doping of $x_c \sim 0.17$ [51]. The AF-I-type magnetic structure is preserved in the low-x regime. At $x \gtrsim 0.04$–0.06, a long-range order (LRO) phase with AF-I type structure is realized below T_N^L, while a short-range order (SRO) phase appears between T_N^S and T_N^L [51]. The ARPES measurements report that the $J_{\text{eff}} = 1/2$ band reaches the Fermi level, forming small hole pockets around the X point at $x \sim 0.07$–0.10 [52,53]. The pseudogaplike behavior is also reported in the hole-doped Sr_2IrO_4 by ARPES [52,53], although there are several distinct differences in the low-energy electronic structure between $Sr_2(Ir_{1-x}Rh_x)O_4$ and electron-doped cuprates.

The phase diagram of cuprates features a plethora of broken symmetries in the pseudogap regime, which

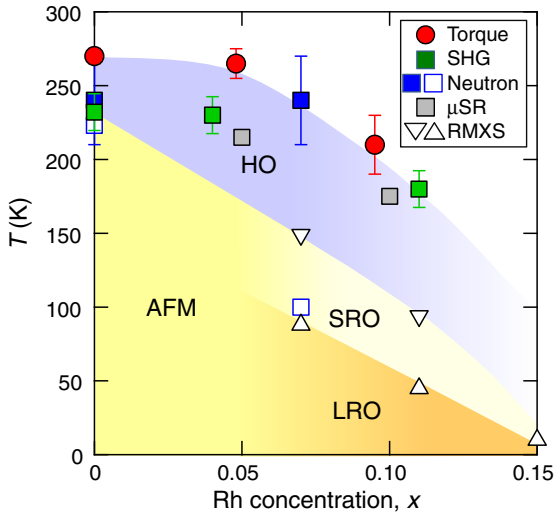

FIG. 3. T–x phase diagram of $Sr_2(Ir_{1-x}Rh_x)O_4$ determined by the SHG, polarized neutron, resonant magnetic x-ray scattering (RMXS) muon spin relaxation, and the present torque measurements. The blue region represents the hidden-order (HO) phase. In the AFM phase, the AF-I magnetic structure at low fields changes to the AF-II structure in parallel fields above about 0.1 T. At $x \gtrsim 0.06$, the magnetic short-range order (SRO) occurs at high temperature, which is followed by magnetic long-range order (LRO) when the AF-II structure occurs.

includes charge-density-wave, stripe, nematic, and possible loop-current orders [54]. Therefore, it is highly intriguing to investigate the symmetry-breaking phase proximate to the spin-orbit coupled Mott insulator Sr_2IrO_4. Recently, the presence of a hidden broken symmetry phase that develops prior to the AFM phase has been reported in pure and Rh-substituted Sr_2IrO_4 by optical second-harmonic generation (SHG) measurements [55]. The SHG can sensitively detect odd-parity order parameters but is insensitive to even-parity order parameters [55–57]. In Fig. 3, the onset temperature of the hidden order determined by the SHG signal T_Ω is plotted. For pure Sr_2IrO_4, T_Ω appears to be a few Kelvin above T_N, and for Rh-doped Sr_2IrO_4, T_Ω is distinctly far above T_N. These results suggest that an odd-parity hidden-order phase develops at higher temperatures above the AFM transition.

Subsequent polarized neutron diffraction measurements in pure and 7% Rh-doped Sr_2IrO_4 report the development of an unconventional magnetic order that breaks time-reversal symmetry above about T_N, which is characterized by an intra-unit-cell magnetic order [58]. The onset temperature of this order matches T_Ω determined by SHG. It should be noted that a similar unconventional magnetic order has been reported in the pseudogap state of underdoped cuprates, including $YBa_2Cu_3O_{6+\delta}$ [18], $HgBa_2CuO_{4+\delta}$ [19], and $Bi_2Sr_2CaCu_2O_y$ [20]. The intra-unit-cell magnetism has been discussed in terms of possible counter-circulating loop currents within the unit cell of IrO_2 or CuO_2 planes (Varma's loop) [12–14]. Very recent muon spin relaxation (μSR) measurements on $Sr_2(Ir_{1-x}Rh_x)O_4$, with $x = 0.05$ and 0.1, report the critical slowing down of electronic spin fluctuations at about T_Ω [59]. Similar phenomena have been reported in the pseudogap state of cuprates [60]. It has been claimed that these muon results are consistent with the polarized neutron experiments. The onset temperatures of the unconventional magnetic order reported by neutron and μSR measurements are plotted in Fig. 3. Since there is no evidence of structural distortions that break translational symmetry above T_N, the hidden-order state is suggested to be a possible anapole state.

Despite the SHG, polarized neutron diffraction, and μSR measurements, however, the nature of the hidden-order state remains largely elusive. To study this state, it is crucially important to clarify the spatial symmetry breaking by a thermodynamic bulk probe. Moreover, although polarized neutron measurements suggest that the direction of the magnetic moment is perpendicular to the ab plane, the direction of the anapole vector is unknown [58]. As there are several patterns of the loop current [12–17], determining the direction of the anapole vector is essentially important for understanding the origin of the broken time-reversal symmetry. In Figs. 4(a) and 4(b), two examples of the anapole vector and loop-current patterns are illustrated.

In this paper, to obtain deep insight into the symmetry-breaking phenomena in the hidden-order phase of $Sr_2(Ir_{1-x}Rh_x)O_4$, we measure the magnetic susceptibility anisotropy within the IrO_2 plane with exceptionally high-precision magnetic torque experiments [61–64] and

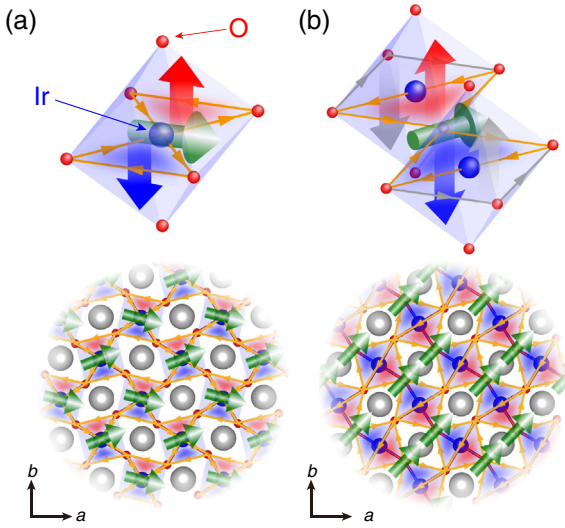

FIG. 4. (a) Upper figure: loop currents (thin orange arrows), induced magnetic fields (thick red and blue arrows), and anapole vector (green arrow) in the IrO_6 octahedron. The net anapole vector is along the [100] Ir-Ir direction. The lower figure is the top view of the upper figure. (b) Same as (a), but the loop current pattern is different. The anapole vector is along the [110] Ir-O-Ir bond direction.

nematic susceptibility with elastoresistance [65–70]. We find that a distinct C_2 in-plane anisotropy that breaks C_4 symmetry of the underlying lattice sets in below about T_Ω in $Sr_2(Ir_{1-x}Rh_x)O_4$. This finding provides thermodynamic evidence for a nematic transition, which bears resemblance to the phenomena observed in the pseudogap state of cuprates [63,64]. However, the nematic director of $Sr_2(Ir_{1-x}Rh_x)O_4$ is along the Ir-O-Ir bond direction, in stark contrast to that of the monolayer cuprate $HgBa_2CuO_{4+\delta}$, which is 45° rotated from the Cu-O-Cu bond direction [64]. Moreover, in contrast to iron-based superconductors, in which the nematic susceptibility is largely enhanced towards the nematic transition [65–69], the nematic susceptibility of $Sr_2(Ir_{1-x}Rh_x)O_4$ exhibits no divergent behavior towards T_Ω, which is consistent with the odd-parity order parameter. Based on these results, we discuss the hidden-order state in terms of an anapole state with peculiar loop-current patterns.

II. EXPERIMENTAL

Measurements of the magnetic torque $\boldsymbol{\tau} = \mu_0 V \boldsymbol{M} \times \boldsymbol{H}$ have a high sensitivity for the detection of magnetic anisotropy, where μ_0 is space permeability, V is the sample volume, and $\boldsymbol{M}$ is the magnetization induced by external magnetic field $\boldsymbol{H}$. Torque is a thermodynamic quantity that is given by the derivative of the free energy with respect to angular displacement, and it can thus shed light on the thermodynamic character of the transition. We perform the torque measurements for a range of directions of $\boldsymbol{H}$ within the tetragonal ab plane of $Sr_2(Ir_{1-x}Rh_x)O_4$ to test whether the hidden-order breaks fourfold crystal symmetry. In this configuration, $\boldsymbol{\tau}$ is a periodic function of twice the azimuthal angle ϕ measured from the a axis:

$$\tau_{2\phi} = \frac{1}{2}\mu_0 V H^2 [(\chi_{aa} - \chi_{bb}) \sin 2\phi - 2\chi_{ab} \cos 2\phi], \quad (1)$$

where χ_{ij} is the susceptibility tensor defined as $M_{ij} = \sum_j \chi_{ij} H_j$ $(i, j = a, b, c)$. For a tetragonally symmetric system, $\tau_{2\phi}$ should be zero because $\chi_{aa} = \chi_{bb}$ and $\chi_{ab} = 0$. Nonzero values of $\tau_{2\phi}$ appear when the tetragonal symmetry is broken by a new electronic or magnetic state; C_4 rotational symmetry breaking is revealed by $\chi_{aa} \neq \chi_{bb}$ and/or $\chi_{ab} \neq 0$. The former and the latter states are illustrated in Figs. 5(a) and 5(b), respectively, where C_4 symmetry breaking occurs along the [100]/[010] direction (B_{1g} symmetry) and the [110] direction (bond-directional nematicity with B_{2g} symmetry) of the IrO_2 plane.

For the in-plane torque magnetometry, we use a highly sensitive piezoresistive cantilever [61–64]. The experimental setup for this measurement is illustrated in Fig. 6(a). To measure the in-plane variation of the magnetic torque, we use a system with two superconducting magnets generating magnetic fields in two mutually orthogonal directions and a cryostat set on a mechanical rotating stage at the top of a dewar [61–64]. By computer-controlling the two superconducting magnets and the rotating stage, $\boldsymbol{H}$ is precisely applied and rotated within the ab plane. We carefully check the misalignment of $\boldsymbol{H}$ from the ab plane by rotating $\boldsymbol{H}$ conically about the c axis and find the misalignment is less than 0.1°. To obtain the maximum torque signal, we apply $\mu_0|\boldsymbol{H}| = 4$ T, which is the highest field available in our vector magnet system. When the nematicity appears in the tetragonal lattice, the formation of nematic domains is naturally expected. In the presence of a large number of domains, the twofold oscillations due to nematicity are canceled out. According to the SHG measurements, the typical domain size is 50–100 μm [55]. Therefore, we use crystals with sizes of less than or about 100 μm in the torque measurements. Since such crystals contain a very small number of domains, the twofold oscillations can be detected if nematicity appears.

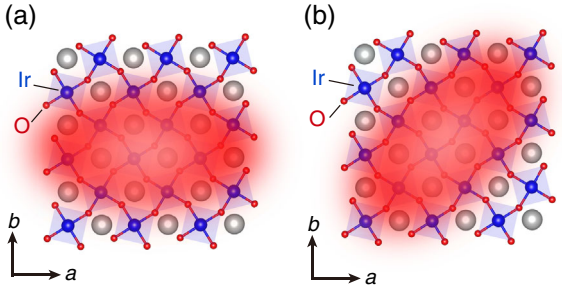

FIG. 5. (a) Schematic picture of the nematicity with B_{1g} symmetry, where the nematic director is along the Ir-Ir [100] direction. For this nematicity, $\chi_{aa} \neq \chi_{bb}$ and $\chi_{ab} = 0$. (b) Nematicity with B_{2g} symmetry, where the nematic director is along the [110] Ir-O-Ir direction. For this nematicity, $\chi_{aa} = \chi_{bb}$ and $\chi_{ab} \neq 0$.

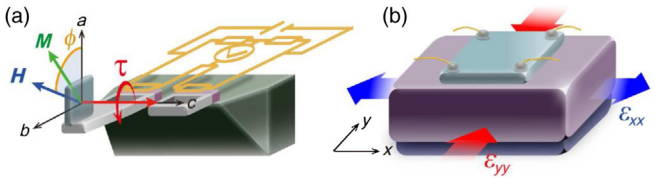

FIG. 6. (a) Experimental setup of in-plane magnetic torque measurements. Magnetic torque $\boldsymbol{\tau} = \mu_0 V \boldsymbol{H} \times \boldsymbol{M}$ is detected by a microcantilever. Here, $\boldsymbol{H}$ is rotated within the ab plane. (b) Experimental setup of elastoresistance measurements. The sample (light blue) is glued on the piezo stack (purple), and the resistances R_{xx} and R_{yy} along the x and y directions, respectively, are measured by the van der Pauw method. The strain ε_{xx} along x is measured by a strain gauge attached on the back side of the piezo stack. The strain ε_{yy} along y is calculated by the temperature-dependent Poisson ratio, which has been calibrated in advance.

The nematic susceptibility is determined by measuring the elastoresistance. The experimental setup for this measurement is illustrated in Fig. 6(b). Two samples are cut from a single crystal of $Sr_2Ir_{0.88}Rh_{0.12}O_4$, and the crystal axes of the samples are determined by x-ray diffraction. Four contacts are attached near the corners of the samples by silver paste and cured at about 250° C. The two samples are glued on the piezo stack, whose x direction is aligned along the [100] and [110] directions, respectively. The van der Pauw method is used to measure resistance changes ΔR_{xx} and ΔR_{yy} along the x and y directions of the piezo stack [67,69]. The difference $\eta = (\Delta R/R)_{xx} - (\Delta R/R)_{yy}$ is the anisotropy induced by the anisotropic strain $\varepsilon_{xx} - \varepsilon_{yy}$, which is measured by the strain gauge. The quantity η is expected to be intimately linked to an electronic nematic-order parameter. When the anisotropic strain couples linearly to the nematic order, the nematic susceptibility can be defined as the quantity

$$\chi_{\rm nem} \equiv d[(\Delta R/R)_{xx} - (\Delta R/R)_{yy}]/d(\varepsilon_{xx} - \varepsilon_{yy}). \quad (2)$$

The measurements of two directions along [100] and [110] correspond to two irreducible representations (B_{1g} and B_{2g}) for the tetragonal D_{4h} system.

III. RESULTS

A. Magnetic torque

Top panels of Figs. 7(a)–7(d) and 7(e)–7(h) display the raw data of the magnetic torque $\tau(\phi)$ in the magnetic field of $\mu_0|\boldsymbol{H}| = 4$ T rotating within the ab plane at several temperatures for pure Sr_2IrO_4 and $Sr_2Ir_{0.905}Rh_{0.095}O_4$ ($T_N^S \approx 120$ K, $T_N^L \approx 80$ K), respectively. Note that we use the unit cell with the space group $I4_1/a$, where the a axis corresponds to the Ir-Ir direction, as shown in Figs. 2(a) and 2(b). This unit cell is 45° rotated from the unit cell of cuprates, where the a axis corresponds to the Cu-O-Cu bond direction. All torque curves are perfectly reversible with respect to the field rotation direction, indicating no detectable ferromagnetic impurities. For both crystals, no oscillations are observed in $\tau(\phi)$ at the highest temperatures, which is consistent with the tetragonal crystal symmetry. At lower temperatures, $\tau(\phi)$ exhibits distinct angular dependence. We analyze $\tau(\phi)$ by decomposing as $\tau = \tau_{2\phi} + \tau_{4\phi}$, where $\tau_{n\phi} = A_{n\phi}\sin[n(\phi - \phi_{n0})]$ is a term with n-fold symmetry. The twofold component is further decomposed as $\tau_{2\phi} = A_{2\phi}^{B1g}\sin 2\phi + A_{2\phi}^{B2g}\cos 2\phi$. In the upper-middle, lower-middle, and bottom panels of Figs. 7(a)–7(h), the B_{2g} twofold, B_{1g} twofold, and fourfold components obtained from the Fourier analysis of the raw

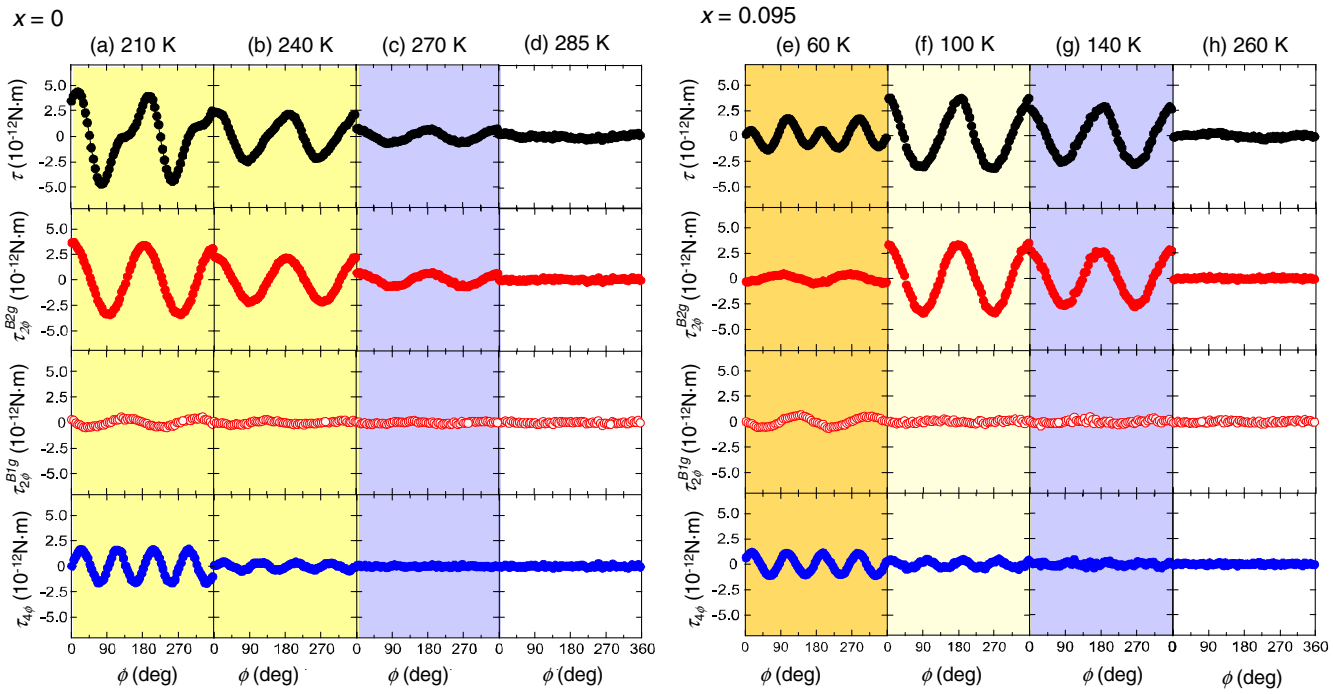

FIG. 7. Rows (a)–(d) and (e)–(h) display the magnetic torque $\tau(\phi)$ in the in-plane magnetic field of $|\mu_0\boldsymbol{H}| = 4$ T as a function of the azimuthal angle ϕ for pure Sr_2IrO_4 ($T_N \approx 240$ K) and $Sr_2Ir_{0.905}Rh_{0.095}O_4$ ($T_N^S \approx 120$ K and $T_N^L \approx 80$ K), respectively. For $x = 0$, white, blue, and yellow shaded regions show that the system is in the paramagnetic, hidden-order, and AFM states, respectively. For $x = 0.095$, the orange (light-yellow) region shows that the system is in the long-range (short-range) AFM state. The top panels show raw torque curves $\tau(\phi)$. The upper-middle, lower-middle, and bottom panels show the B_{2g} twofold ($\cos 2\phi$), B_{1g} twofold ($\sin 2\phi$), and fourfold ($\sin 4\phi$) components of the torque curves, respectively, obtained from Fourier analysis of the raw torque curves.

torque curves are displayed. The raw $\tau(\phi)$ curves are well reproduced by the sum of these three components.

As shown in the upper middle panels of Figs. 7(a)–7(g), distinct twofold oscillation with B_{2g} symmetry ($\propto \cos 2\phi$) is observed at 270 K for Sr_2IrO_4 and at 140 K for $Sr_2Ir_{0.905}Rh_{0.095}O_4$. It should be stressed that these temperatures are obviously higher than T_N. Therefore, the data provide the first evidence for a phase transition to an electronic nematic state as a bulk property. As shown in the lower-middle and bottom panels of Figs. 7(a)–7(h), small but finite twofold oscillations with B_{1g} symmetry ($\propto \sin 2\phi$) and fourfold oscillations, which have the form $\tau_{4\phi} = A_{4\phi} \sin 4\phi$, are observed at low temperatures.

Figures 8(a)–8(c) depict the temperature dependence of the amplitude of each oscillation for $Sr_2(Ir_{1-x}Rh_x)O_4$, with $x = 0$ (pure), 0.048, and 0.095, respectively. In all crystals, finite twofold B_{2g} oscillations appear well above T_N or T_N^S. Moreover, the amplitude of twofold oscillations grows nearly linearly with decreasing temperature as $A_{2\phi}^{B2g} \propto |T_\Omega - T|^\beta$, with $\beta \approx 1$. The onset temperature of the twofold B_{2g} oscillations is plotted in the T–x phase diagram displayed in Fig. 3. We note that the onset temperature of the twofold B_{2g} oscillations does not depend on the magnetic field strength. For pure Sr_2IrO_4, the onset temperature of twofold B_{2g} oscillations is slightly higher than the onset temperatures reported by the SHG and polarized neutron scattering measurements [55,58]. In Rh-doped Sr_2IrO_4, on the other hand, the onset temperature appears to be close to that determined by the SHG and neutron measurements. Considering the ambiguity in determining the onset temperature of the SHG signal and the neutron diffraction intensity, the onset temperature of the tetragonal C_4 symmetry breaking appears to match that of the hidden-order T_Ω. Thus, the present results provide thermodynamic evidence of the nematic transition at about T_Ω.

For pure Sr_2IrO_4 and $x = 0.048$, $A_{2\phi}^{B2g}(T)$ increases with decreasing temperature with no discernible change at T_N and shows a saturating behavior at lower temperatures. These results suggest that the nematicity is insensitive to the long-range AFM order. In contrast, for 0.095, $A_{2\phi}^{B2g}(T)$ is strongly suppressed below about T_N^S and changes sign below T_N^L, suggesting that the B_{2g} nematicity is strongly influenced by the appearance of short-range magnetic structure. With decreasing temperature, the amplitude of fourfold oscillations increases below T_N for pure Sr_2IrO_4 [71,72]. The torque curves are perfectly reversible with respect to the field rotation below T_N, indicating that the induced weak ferromagnetic moments completely follow the applied $\boldsymbol{H}$ rotated within the ab plane. Moreover, the fourfold oscillations for $x = 0.048$ and 0.095 appear even above the AFM-ordering temperatures. These results indicate that the fourfold oscillations are not caused by the weak ferromagnetic moments shown in Fig. 2(d) but arise primarily from the nonlinear susceptibilities [61].

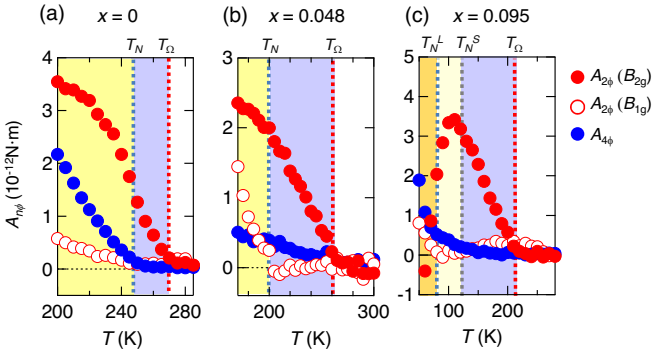

FIG. 8. Temperature dependence of the amplitude of twofold (red filled and open circles) and fourfold oscillations (filled blue circles) for pure and Rh-doped Sr_2IrO_4. (a) $x = 0$, (b) $x = 0.048$, and (c) $x = 0.095$.

B. Elastoresistance

The elastoresistance measurements have been used as a powerful probe of electronic nematic transitions in strongly correlated electron systems, especially in iron-based superconductors [65,66,68,69,73]. When the nematic order couples linearly to the strain, this technique can quantify the nematic susceptibility, which is related to the fluctuations of a rotational-symmetry-breaking order above the nematic transition. Thus, this method is complementary to the magnetic torque measurements, which measure the nematic-order parameter below the transition.

The results of elastoresistance measurements along two different strain directions are shown in Figs. 9(a)–(d). The linearity of the resistance change with respect to the strain observed for both x and y directions indicates that the anisotropy η is proportional to the strain. The doping level of the samples is $x = 0.12$, where the long-range antiferromagnetic and hidden-order transition temperatures are expected to be about 30 K and 150 K (see Fig. 3). As shown in Fig. 10(a), the temperature dependence of the nematic susceptibility $\chi_{\rm nem} = d[(\Delta R/R)_{xx} - (\Delta R/R)_{yy}]/d(\varepsilon_{xx} - \varepsilon_{yy})$ along [100] shows a gradual increase with decreasing temperature, but it does not show any divergent behavior near the putative hidden-order transition around 150 K. The data for the [110] direction [Fig. 10(b)], which is along the nematic director expected from the torque measurements, show even weaker temperature dependence with no discernible anomaly around 150 K. In both directions, an enhancement is observed below 30 K below the Néel temperature T_N^L, where the ground state is insulating. The observed absence of the divergent behavior in two directions, which correspond to two irreducible representations B_{1g} and B_{2g} in the tetragonal D_{4h} system, provides evidence against even-parity nematic order in the hidden-order phase of $Sr_2Ir_{1-x}Rh_xO_4$. Therefore, this evidence implies that the rotational symmetry-breaking

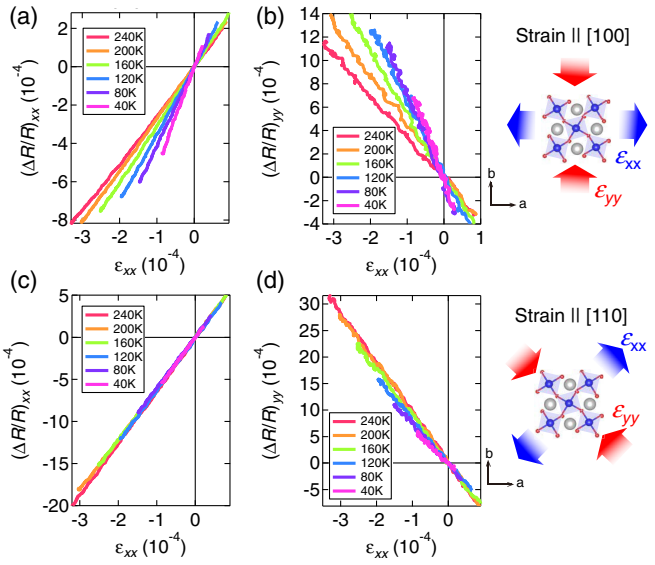

FIG. 9. Representative data of elastoresistance for $Sr_2(Ir_{1-x}Rh_x)O_4$ with $x = 0.12$. (a) Longitudinal elastoresistance $(\Delta R/R)_{xx}$ and (b) transverse elastoresistance $(\Delta R/R)_{yy}$ for several temperatures as a function of strain ε_{xx} with the strain direction x parallel to [100]. (c) Longitudinal elastoresistance $(\Delta R/R)_{xx}$ and (d) transverse elastoresistance $(\Delta R/R)_{yy}$ for several temperatures as a function of strain ε_{xx} with the strain direction x parallel to [110]. The linear response of the resistance against the strain can be seen in all the elastoresistance data.

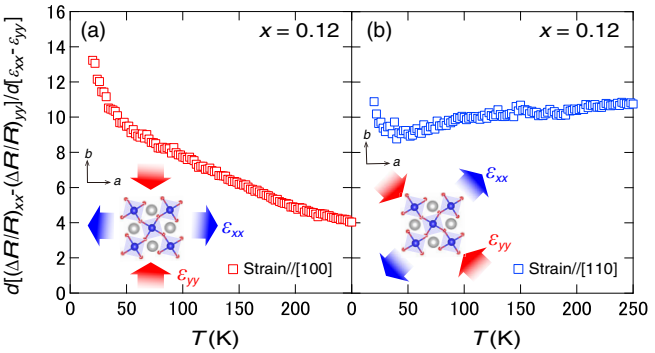

FIG. 10. Temperature dependence of nematic susceptibility in $Sr_2Ir_{0.88}Rh_{0.12}O_4$. (a) Strain applied along the [100] direction. (b) Strain applied along the [110] direction. The insets illustrate the directions of applied strain and the IrO_6 octahedra.

state revealed by the magnetic torque is of odd parity, as will be discussed later.

IV. DISCUSSION

Our main experimental findings for pure and Rh-substituted Sr_2IrO_4 are threefold: First, the in-plane torque magnetometry provides thermodynamic evidence of the nematic transition that lowers the rotational symmetry of the system from C_4 to C_2 at about T_Ω. Second, the growth of B_{2g} twofold oscillations indicates a nematic director along the Ir-O-Ir [110] bond direction, in contrast to previous proposals [55,58]. Third, the elastoresistance shows no diverging nematic susceptibility towards T_Ω. We note that the possibility of the field-induced twofold oscillations in the paramagnetic phase can be excluded because of the following reason: When the in-plane anisotropy is induced by the external magnetic field, the direction of the anisotropy is expected to follow the rotation of the magnetic field. Therefore, the field-induced anisotropy, even if present, does not induce the twofold oscillations in the paramagnetic phase above T_N. Moreover, we point out that these results are consistent with the anapole state, which has been proposed by SHG and polarized neutron measurements [55,58]. It should be noted that the anapole-order parameter breaks inversion symmetry while the magnetic field preserves it. Thus, the coupling between the anapole moment and external magnetic field is not linear but arises from a second-order effect. This coupling gives rise to twofold magnetic anisotropy, which is detected as a twofold oscillation of the in-plane magnetic torque. Moreover, below T_Ω, the amplitude of the twofold oscillations increases nearly linearly, which implies that the nematicity is not a primary order parameter but a secondary one of the hidden-order state.

In Fe-based superconductors, including $Ba(Fe_{1-x}Co_x)_2As_2$, $BaFe_2(As_{1-x}P_x)_2$, and $FeSe_{1-x}S_x$, the nematic susceptibility exhibits diverging behavior toward the nematic transition temperature [65,66,68]. In addition, the divergent nematic susceptibility has also been reported in a cuprate $(Bi,Pb)_2Sr_2CaCu_2O_{8+\delta}$ near the pseudogap critical point [70]. Therefore, the absence of the divergent nematic susceptibility with approaching T_Ω, despite the presence of a thermodynamic nematic transition, is in sharp contrast to the nematic transition reported in other strongly correlated electron systems. One may suspect that electrons couple with the lattice very weakly in $Sr_2(Ir_{1-x}Rh_x)O_4$. However, such a possibility is unlikely because the inherently strong spin-orbit interaction in $Sr_2(Ir_{1-x}Rh_x)O_4$ is expected to give rise to a strong coupling between the electrons and the lattice. The present results of $Sr_2(Ir_{1-x}Rh_x)O_4$ suggest that the hidden-order state is not a simple ferroic nematic-ordered phase characterized by the wave vector $\boldsymbol{q} = 0$.

We stress that the absence of divergent nematic susceptibility is consistent with the odd-parity order for the following reasons. In the case of even-parity ferroic nematic order, the elastoresistance measurements can sensitively detect the divergent behavior of nematic susceptibility toward the transition temperature. If the order is of odd parity, on the other hand, the divergence may not be observed from the elastoresistance because the linear coupling between the strain and the odd-parity order parameter is prohibited. In fact, in the Landau theory, coupling of anapole order and strain is described as

$$F = F_{\mathrm{lat}} + F_{\mathrm{ana}} + \gamma_1 T_x T_y \varepsilon_{xy} + \gamma_2 (T_x^2 - T_y^2)(\varepsilon_{xx} - \varepsilon_{yy}), \quad (3)$$

where $\boldsymbol{T} = (T_x, T_y)$ is a polar-vector order parameter for the anapole order in the E_u representation, ε_{ij} are strain, γ_1 and γ_2 are coupling constants, and F_{lat} and F_{ana} are the free energy of the lattice strain and anapole order, respectively. Any linear coupling of the anapole-order parameter and strain, $T_i \varepsilon_{jk}$, is prohibited because T_i and ε_{jk} have different spacial inversion and time-reversal symmetries; anapole order is odd parity while the strain is even parity. The absence of the linear couplings reveals no divergent susceptibility when approaching the anapole transition T_Ω from high temperatures, which is in contrast to the even-parity nematic case whose order parameters couple linearly to the strain. On the other hand, the bond-directional anapole-order parameter grows below T_Ω as $|T_x| = |T_y| \propto (T_\Omega - T)^{1/2}$ in the mean field region. Through the coupling term in Landau free energy, nematicity $\varepsilon_{xy} \propto T_\Omega - T$ is induced below T_Ω. These expected behaviors in the mean field region of anapole order are compatible with the results of magnetic torque and elastoresistance measurements.

We now discuss the direction of the anapole moment and loop-current pattern in the hidden-order state. The polar toroidal moment that points to the a axis and the simplest loop-current pattern illustrated in Fig. 4(a) have been proposed in the previous SHG and polarized neutron diffraction studies [55,58]. In our torque magnetometry, however, the twofold oscillations below T_Ω follow the functional form $\tau_{2\phi} = A_{2\phi} \cos 2\phi$. This result clearly indicates $\chi_{aa} = \chi_{bb}$ and $\chi_{ab} \neq 0$ in Eq. (1), i.e., the emergence of the nematicity whose anisotropy axis is along the Ir-O-Ir direction, which is referred to as bond nematicity. The direction of the nematic director is the same as that of the anapole moment. Therefore, the torque magnetometry reveals that the anapole moment points to the [110] direction and rotated 45° from the a axis, as illustrated in Fig. 4(b).

Among the resemblances of crystallographic, magnetic, and electronic structures between Sr_2IrO_4 and La_2CuO_4, the formation of a pseudogap with the Fermi arc in electron-doped Sr_2IrO_4 has drawn a great deal of attention because the pseudogap is one of the most prominent and most discussed features of the cuprates. The hole doping in the iridate is roughly equivalent to the electron doping in cuprates. Nevertheless, we suggest that the symmetry-breaking phenomena in the hidden-order phase of Rh-doped Sr_2IrO_4 bear a striking resemblance to those in the pseudogap phase in hole-doped cuprates. In particular, the emergence of rotational symmetry breaking is a remarkable common feature of two different Mott insulating systems. Thus, detailed comparisons of the nematicity between the cuprates and the iridate could reveal important information on the peculiar electronic properties of both systems.

It has been reported that the nematic director in $YBa_2Cu_3O_{6+\delta}$ and $(Bi,Pb)_2Sr_2CaCu_2O_{8+\delta}$ orients along the Cu-O-Cu bond direction [63,74], while it orients along the diagonal direction of the CuO_2 square lattice in $HgBa_2CuO_{4+\delta}$ [64]. Although the difference of the nematic direction among cuprates remains an open question, it may be due to the number of CuO_2 planes in the unit cell [21]. Therefore, the comparison between the monolayer cuprate $HgBa_2CuO_{4+\delta}$ and the single layered iridate Sr_2IrO_4 is more relevant. In $HgBa_2CuO_{4+\delta}$, polarized neutron diffraction experiments have revealed an unusual $\boldsymbol{q} = 0$ magnetic order below the pseudogap temperature, which has been discussed in terms of loop-current-like magnetism breaking both time-reversal and parity symmetries [19,75,76]. The in-plane torque magnetometry in $HgBa_2CuO_{4+\delta}$ reported that the nematic director orients along the diagonal direction of the CuO_2 square lattice, whereas neutron scattering experiments reported that the loop currents in $HgBa_2CuO_{4+\delta}$ are not only oriented diagonally but are also out of plane [76]. Although both in-plane torque and nematic susceptibility measurements are insensitive to the out-of-plane properties, we point out that the nematic director in the hidden-order phase of Sr_2IrO_4 is rotated 45° from that in the pseudogap state of $HgBa_2CuO_{4+\delta}$ in the basal plane. Therefore, if the loop-current-like magnetism is an origin of the nematicity, the loop-current pattern of Sr_2IrO_4, which is illustrated in Fig. 4(b), must be different from that of $HgBa_2CuO_{4+\delta}$. Our results show that the intra-unit-cell loop current flows only in one of the diagonal directions in the IrO_4 square in both pure and Rh-doped Sr_2IrO_4 [15–17].

The interpretation of the twofold oscillations in the AFM-ordered states is rather complicated. The rapid suppression of the amplitude of twofold oscillations with B_{2g} symmetry below T_N^S may be due to the segmentation of the domain structure by short-range magnetic order. A further detailed study is required to clarify how the short-range magnetic order influences the anapole moment. As shown in Figs. 8(a)–8(c), two-fold oscillations with B_{1g} symmetry appear below the long-range AFM-ordering temperatures, which may be due to the coupling between the pseudospin and the lattice [77].

V. CONCLUSIONS

In summary, we measured the in-plane magnetic torque and elastoresistance in a spin-orbit coupled Mott insulator $Sr_2(Ir_{1-x}Rh_x)O_4$. The measurements of in-plane anisotropy of the magnetic susceptibility reveal the emergence of the nematic phase with broken rotation symmetry distinctly above the Néel transition. On the other hand, nematic susceptibility exhibits no diverging behavior when approaching the nematic critical point. These results provide bulk evidence for the odd-parity hidden-order state suggested by the SHG. The results, along with the report of polarized neutron diffraction, suggest that the hidden-order

phase is in an anapole state, which is composed of a polar (magnetic) toroidal dipole induced by persistent loop currents. These results may bear a resemblance to the pseudogap state of underdoped cuprates, but the nematic director of $Sr_2(Ir_{1-x}Rh_x)O_4$ is rotated 45° from that of the monolayer cuprate $HgBa_2CuO_{4+\delta}$, implying the difference of the loop-current patterns between the two systems. The remarkable common features of the nematicity and distinct differences of the nematic director may be key to understanding the symmetry-breaking phenomena in the hidden-order state of the iridate and the pseudogap state of the cuprates.

ACKNOWLEDGMENTS

We thank T. Kimura, H. Kontani, and E.-G. Moon for discussions. This work is supported by Grants-in-Aid for Scientific Research (KAKENHI) (No. JP18H01177, No. JP18H01178, No. JP18H01180, No. JP18H05227, No. JP18K13492, No. JP19H00649, No. JP20H02600, No. JP20H05159, and No. JP20K21139) and on Innovative Areas "Quantum Liquid Crystals" (No. JP19H05824) from Japan Society for the Promotion of Science (JSPS), and JST CREST (JPMJCR19T5). G. C. acknowledges NSF support via Grant No. DMR 1903888.

[1] N. A Spaldin, M. Fiebig, and M. Mostovoy, *The Toroidal Moment in Condensed-Matter Physics and Its Relation to the Magnetoelectric Effect*, J. Phys. Condens. Matter **20**, 434203 (2008).

[2] S. Nanz, *Multipole Expansion of the Potentials: Toroidal Multipole Moments in Classical Electrodynamics—An Analysis of Their Emergence and Physical Significance* (Springer Spektrum, Wiesbaden, 2016).

[3] S. Gnewuch and E. E. Rodriguez, *The Fourth Ferroic Order: Current Status on Ferrotoroidic Materials*, J. Solid State Chem. **271**, 175 (2019).

[4] V. M. Dubovik, L. A. Tosunyan, and V. V. Tugushev, *Axial Toroidal Moments in Electrodynamics and Solid-State Physics*, JETP Lett. **63**, 344 (1986).

[5] V. M. Dubovik and V. V. Tugushev, *Toroid Moments in Electrodynamics and Solid-State Physics*, Phys. Rep. **187**, 145 (1990).

[6] A. K. Yadav, C. T. Nelson, S. L. Hsu, Z. Hong, J. D. Clarkson, C. M. Schlepütz, A. R. Damodaran, P. Shafer, E. Arenholz, L. R. Dedon, D. Chen, A. Vishwanath, A. M. Minor, L. Q. Chen, J. F. Scott, L. W. Martin, and R. Ramesh, *Observation of Polar Vortices in Oxide Superlattices*, Nature (London) **530**, 198 (2016).

[7] W. Jin, E. Drueke, S. Li, A. Admasu, R. Owen, M. Day, K. Sun, S.-W. Cheong, and L. Zhao, *Observation of a Ferro-rotational Order Coupled with Second-Order Nonlinear Optical Fields*, Nat. Phys. **16**, 42 (2020).

[8] A. Nakano, T. Hasegawa, S. Tamura, N. Katayama, S. Tsutsui, and H. Sawa, *Antiferroelectric Distortion with Anomalous Phonon Softening in the Excitonic Insulator,* Ta_2NiSe_5, Phys. Rev. B **98**, 045139 (2018).

[9] B. B. Van Aken, J.-P. Rivera, H. Schmid, and M. Fiebig, *Observation of Ferrotoroidic Domains*, Nature (London) **449**, 702 (2007).

[10] V. Scagnoli, U. Staub, Y. Bodenthin, R. A. de Souza, M. García-Fernández, M. Garganourakis, A. T. Boothroyd, D. Prabhakaran, and S. W. Lovesey, *Observation of Orbital Currents in CuO*, Science **332**, 696 (2011).

[11] S. Di Matteo and M. R. Norman, *Orbital Currents, Anapoles, and Magnetic Quadrupoles in CuO*, Phys. Rev. B **85**, 235143 (2012).

[12] C. M. Varma, *Theory of the Pseudogap State of the Cuprates*, Phys. Rev. B **73**, 155113 (2006).

[13] C. M. Varma, *Pseudogap in Cuprates in the Loop-Current Ordered State*, J. Phys. Condens. Matter **26**, 505701 (2014).

[14] S. S. Pershoguba, K. Kechedzhi, and V. M. Yakovenko, *Proposed Chiral Texture of the Magnetic Moments of Unit-Cell Loop Currents in the Pseudogap Phase of Cuprate Superconductors*, Phys. Rev. Lett. **111**, 047005 (2013); S. S. Pershoguba, K. Kechedzhi, and V. M. Yakovenko, *Erratum: Proposed Chiral Texture of the Magnetic Moments of Unit-Cell Loop Currents in the Pseudogap Phase of Cuprate*, Phys. Rev. Lett. **113**, 129901 (2014).

[15] S. Chatterjee, S. Sachdev, and M. S. Scheurer, *Intertwining Topological Order and Broken Symmetry in a Theory of Fluctuating Spin-Density Waves*, Phys. Rev. Lett. **119**, 227002 (2017).

[16] M. S. Scheurer and S. Sachdev, *Orbital Currents in Insulating and Doped Antiferromagnets*, Phys. Rev. B **98**, 235126 (2018).

[17] S. Sachdev, H. D. Scammell, M. S. Scheurer, and G. Tarnopolsky, *Gauge Theory for the Cuprates Near Optimal Doping*, Phys. Rev. B **99**, 054516 (2019).

[18] B. Fauqué, Y. Sidis, V. Hinkov, S. Pailheś, C. T. Lin, X. Chaud, and P. Bourges, *Magnetic Order in the Pseudogap Phase of High-*T_c *Superconductors*, Phys. Rev. Lett. **96**, 197001 (2006).

[19] Y. Li, V. Balédent, N. Barišić, Y. Cho, B. Fauqué, Y. Sidis, G. Yu, X. Zhao, P. Bourges, and M. Greven, *Unusual Magnetic Order in the Pseudogap Region of the Superconductor* $HgBa_2CuO_{4+\delta}$, Nature (London) **455**, 372 (2008).

[20] S. De Almeida-Didry, Y. Sidis, V. Baledent, F. Giovannelli, I. Monot-Laffez, and P. Bourges, *Evidence for Intra-Unit-Cell Magnetic Order in* $Bi_2Sr_2CaCu_2O_{8+\delta}$, Phys. Rev. B **86**, 020504(R) (2012).

[21] L. Mangin-Thro, Y. Li, Y. Sidis, and P. Bourges, $a-b$ *Anisotropy of the Intra-Unit-Cell Magnetic Order in* $YBa_2Cu_3O_{6.6}$, Phys. Rev. Lett. **118**, 097003 (2017).

[22] T. P. Croft, E. Blackburn, J. Kulda, R. Liang, D. A. Bonn, W. N. Hardy, and S. M. Hayden, *No Evidence for Orbital Loop Currents in Charge-Ordered* $YBa_2Cu_3O_{6+x}$ *from Polarized Neutron Diffraction*, Phys. Rev. B **96**, 214504 (2017).

[23] P. Bourges, Y. Sidis, and L. Mangin-Thro, *Comment on "No Evidence for Orbital Loop Currents in Charge-Ordered* $YBa_2Cu_3O_{6+x}$ *from Polarized Neutron Diffraction*, Phys. Rev. B **98**, 016501 (2018).

[24] T. P. Croft, E. Blackburn, J. Kulda, R. Liang, D. A. Bonn, W. N. Hardy, and S. M. Hayden, *Reply to "Comment on 'No Evidence for Orbital Loop Currents in Charge-Ordered* $YBa_2Cu_3O_{6+x}$ *from Polarized Neutron Diffraction,'"* Phys. Rev. B **98**, 016502 (2018).

[25] B. J. Kim, H. Jin, S. J. Moon, J.-Y. Kim, B.-G. Park, C. S. Leem, J. Yu, T. W. Noh, C. Kim, S.-J. Oh, J.-H. Park, V. Durairaj, G. Cao, and E. Rotenberg, *Novel* $J_{\mathrm{eff}} = 1/2$ *Mott State Induced by Relativistic Spin-Orbit Coupling in* Sr_2IrO_4, Phys. Rev. Lett. **101**, 076402 (2008).

[26] J. G. Rau, E. K. -H. Lee, and H. Y. Kee, *Spin-Orbit Physics Giving Rise to Novel Phases in Correlated Systems: Iridates and Related Materials*, Annu. Rev. Condens. Matter Phys. **7**, 195 (2016).

[27] G. Cao and P. Schlottmann, *The Challenge of Spin-Orbit-Tuned Ground States in Iridates: A Key Issues Review*, Rep. Prog. Phys. **81**, 042502 (2018).

[28] J. Bertinshaw, Y. K. Kim, G. Khaliullin, and B. J. Kim, *Square Lattice Iridates*, Annu. Rev. Condens. Matter Phys. **10**, 315 (2019).

[29] J. Dai, E. Calleja, G. Cao, and K. McElroy, *Local Density of States Study of a Spin-Orbit-Coupling Induced Mott Insulator* Sr_2IrO_4, Phys. Rev. B **90**, 041102(R) (2014).

[30] M. K. Crawford, M. A. Subramanian, R. L. Harlow, J. A. Fernandez-Baca, Z. R. Wang, and D. C. Johnston, *Structural and Magnetic Studies of* Sr_2IrO_4, Phys. Rev. B **49**, 9198 (1994).

[31] C. Dhital, T. Hogan, Z. Yamani, C. de la Cruz, X. Chen, S. Khadka, Z. Ren, and S. D. Wilson, *Neutron Scattering Study of Correlated Phase Behavior in* Sr_2IrO_4, Phys. Rev. B **87**, 144405 (2013).

[32] F. Ye, S. Chi, B. C. Chakoumakos, J. A. Fernandez-Baca, T. Qi, and G. Cao, *Magnetic and Crystal Structures of* Sr_2IrO_4*: A Neutron Diffraction Study*, Phys. Rev. B **87**, 140406(R) (2013).

[33] D. H. Torchinsky, H. Chu, L. Zhao, N. B. Perkins, Y. Sizyuk, T. Qi, G. Cao, and D. Hsieh, *Structural Distortion-Induced Magnetoelastic Locking in* Sr_2IrO_4 *Revealed through Nonlinear Optical Harmonic Generation*, Phys. Rev. Lett. **114**, 096404 (2015).

[34] B. J. Kim, H. Ohsumi, T. Komesu, S. Sakai, T. Morita, H. Takagi, and T. Arima, *Phase-Sensitive Observation of a Spin-Orbital Mott State in* Sr_2IrO_4, Science **323**, 1329 (2009).

[35] S. Boseggia, H. C. Walker, J. Vale, R. Springell, Z. Feng, R. S. Perry, M. M. Sala, H. M. Rønnow, S. P. Collins, and D. F. McMorrow, *Locking of Iridium Magnetic Moments to the Correlated Rotation of Oxygen Octahedra in* Sr_2IrO_4 *Revealed by X-Ray Resonant Scattering*, J. Phys. Condens. Matter **25**, 422202 (2013).

[36] J. Kim, D. Casa, M. H. Upton, T. Gog, Y.-J. Kim, J. F. Mitchell, M. van Veenendaal, M. Daghofer, J. van den Brink, G. Khaliullin, and B. J. Kim, *Magnetic Excitation Spectra of* Sr_2IrO_4 *Probed by Resonant Inelastic X-Ray Scattering: Establishing Links to Cuprate Superconductors*, Phys. Rev. Lett. **108**, 177003 (2012).

[37] F. Wang and T. Senthil, *Twisted Hubbard Model for* Sr_2IrO_4*: Magnetism and Possible High Temperature Superconductivity*, Phys. Rev. Lett. **106**, 136402 (2011).

[38] M. Ge, T. F. Qi, O. B. Korneta, D. E. De Long, P. Schlottmann, W. P. Crummett, and G. Cao, *Lattice-Driven Magnetoresistivity and Metal-Insulator Transition in Single-Layered Iridates*, Phys. Rev. B **84**, 100402(R) (2011).

[39] X. Chen, T. Hogan, D. Walkup, W. Zhou, M. Pokharel, M. Yao, W. Tian, T. Z. Ward, Y. Zhao, D. Parshall, C. Opeil, J. W. Lynn, V. Madhavan, and S. D. Wilson, *Influence of Electron Doping on the Ground State of* $(Sr_{1-x}La_x)_2IrO_4$, Phys. Rev. B **92**, 075125 (2015).

[40] Y. K. Kim, O. Krupin, J. D. Denlinger, A. Bostwick, E. Rotenberg, Q. Zhao, J. F. Mitchell, J. W. Allen, and B. J. Kim, *Fermi Arcs in a Doped Pseudospin-*$1/2$ *Heisenberg Antiferromagnet*, Science **345**, 187 (2014).

[41] Y. K. Kim, N. H. Sung, J. D. Denlinger, and B. J. Kim, *Observation of a d-Wave Gap in Electron-Doped* Sr_2IrO_4, Nat. Phys. **12**, 37 (2016).

[42] V. Brouet, J. Mansart, L. Perfetti, C. Piovera, I. Vobornik, P. Le Fèvre, F. Bertran, S. C. Riggs, M. C. Shapiro, P. Giraldo-Gallo, and I. R. Fisher, *Transfer of Spectral Weight Across the Gap of* Sr_2IrO_4 *Induced by La Doping*, Phys. Rev. B **92**, 081117(R) (2015).

[43] A. de la Torre, S. M. Walker, F. Y. Bruno, S. Riccó, Z. Wang, I. G. Lezama, G. Scheerer, G. Giriat, D. Jaccard, C. Berthod, T. K. Kim, M. Hoesch, E. C. Hunter, R. S. Perry, A. Tamai, and F. Baumberger, *Collapse of the Mott Gap and Emergence of a Nodal Liquid in Lightly Doped* Sr_2IrO_4, Phys. Rev. Lett. **115**, 176402 (2015).

[44] Y. J. Yan, M. Q. Ren, H. C. Xu, B. P. Xie, R. Tao, H. Y. Choi, N. Lee, Y. J. Choi, T. Zhang, and D. L. Feng, *Electron-Doped* Sr_2IrO_4*: An Analogue of Hole-Doped Cuprate Superconductors Demonstrated by Scanning Tunneling Microscopy*, Phys. Rev. X **5**, 041018 (2015).

[45] I. Battisti, K. M. Bastiaans, V. Fedoseev, A. de la Torre, N. Iliopoulos, A. Tamai, E. C. Hunter, R. S. Perry, J. Zaanen, F. Baumberger, and M. P. Allan, *Universality of Pseudogap and Emergent Order in Lightly Doped Mott Insulators*, Nat. Phys. **13**, 21 (2017).

[46] H. Watanabe, T. Shirakawa, and S. Yunoki, *Monte Carlo Study of an Unconventional Superconducting Phase in Iridium Oxide* $J_{\mathrm{eff}} = 1/2$ *Mott Insulators Induced by Carrier Doping*, Phys. Rev. Lett. **110**, 027002 (2013).

[47] Y. Yang, W.-S. Wang, J.-G. Liu, H. Chen, J.-H. Dai, and Q.-H. Wang, *Superconductivity in Doped* Sr_2IrO_4*: A Functional Renormalization Group Study*, Phys. Rev. B **89**, 094518 (2014).

[48] Z. Y. Meng, Y. B. Kim, and H.-Y. Kee, *Odd-Parity Triplet Superconducting Phase in Multiorbital Materials with a Strong Spin-Orbit Coupling: Application to Doped* Sr_2IrO_4, Phys. Rev. Lett. **113**, 177003 (2014).

[49] T. F. Qi, O. B. Korneta, L. Li, K. Butrouna, V. S. Cao, X. Wan, P. Schlottmann, R. K. Kaul, and G. Cao, *Spin-Orbit Tuned Metal-Insulator Transitions in Single-Crystal* $Sr_2(Ir_{1-x}Rh_x)O_4$ $(0 \le x \le 1)$, Phys. Rev. B **86**, 125105 (2012).

[50] F. Ye, X. Wang, C. Hoffmann, J. Wang, S. Chi, M. Matsuda, B. C. Chakoumakos, J. A. Fernandez-Baca, and G. Cao, Structure Symmetry Determination and Magnetic Evolution in $Sr_2(Ir_{1-x}Rh_x)O_4$, Phys. Rev. B **92**, 201112(R) (2015).

[51] J. P. Clancy, A. Lupascu, H. Gretarsson, Z. Islam, Y. F. Hu, D. Casa, C. S. Nelson, S. C. LaMarra, G. Cao, and Y.-J. Kim, *Dilute Magnetism and Spin-Orbital Percolation Effects in* $Sr_2(Ir_{1-x}Rh_x)O_4$, Phys. Rev. B **89**, 054409 (2014).

[52] Y. Cao, Q. Wang, J. A. Waugh, T. J. Reber, H. Li, X. Zhou, S. Parham, S.-R. Park, N. C. Plumb, E. Rotenberg, A. Bostwick, J. D. Denlinger, T. Qi, M. A. Hermele, G. Cao, and D. S. Dessau, *Hallmarks of the Mott-Metal Crossover in the Hole-Doped Pseudospin-*$1/2$ *Mott Insulator* Sr_2IrO_4, Nat. Commun. **7**, 11367 (2016).

[53] A. Louat, F. Bert, L. Serrier-Garcia, F. Bertran, P. Le Fèvre, J. Rault, and V. Brouet, *Formation of an Incoherent Metallic State in Rh-Doped* Sr_2IrO_4, Phys. Rev. B **97**, 161109(R) (2018).

[54] B. Keimer, S. A. Kivelson, M. R. Norman, S. Uchida, and J. Zaanen, *From Quantum Matter to High-Temperature Superconductivity in Copper Oxides*, Nature (London) **518**, 179 (2015).

[55] L. Zhao, D. H. Torchinsky, H. Chu, V. Ivanov, R. Lifshitz, R. Flint, T. Qi, G. Cao, and D. Hsieh, *Evidence of an Odd-Parity Hidden Order in a Spin-Orbit Coupled Correlated Iridate*, Nat. Phys. **12**, 32 (2016).

[56] L. Zhao, C. A. Belvin, R. Liang, D. A. Bonn, W. N. Hardy, N. P. Armitage, and D. Hsieh, *A Global Inversion-Symmetry-Broken Phase Inside the Pseudogap Region of* $YBa_2Cu_3O_y$, Nat. Phys. **13**, 250 (2017).

[57] J. W. Harter, Z. Y. Zhao, J.-Q. Yan, D. G. Mandrus, and D. Hsieh, *A Parity-Breaking Electronic Nematic Phase Transition in the Spin-Orbit Coupled Metal* $Cd_2Re_2O_7$, Science **356**, 295 (2017).

[58] J. Jeong, Y. Sidis, A. Louat, V. Brouet, and P. Bourges, *Time-Reversal Symmetry Breaking Hidden Order in* $Sr_2(Ir, Rh)O_4$, Nat. Commun. **8**, 15119 (2017).

[59] C. Tan, Z. F. Ding, J. Zhang, Z. H. Zhu, O. O. Bernal, P. C. Ho, A. D. Hillier, A. Koda, H. Luetkens, G. D. Morris, D. E. MacLaughlin, and L. Shu, *Slow Magnetic Fluctuations and Critical Slowing Down in* $Sr_2(Ir_{1-x}Rh_x)O_4$, Phys. Rev. B **101**, 195108 (2020).

[60] J. Zhang, Z. Ding, C. Tan, K. Huang, O. O. Bernal, P.-C. Ho, G. D. Morris, A. D. Hillier, P. K. Biswas, S. P. Cottrell, H. Xiang, X. Yao, D. E. MacLaughlin, and L. Shu, *Discovery of Slow Magnetic Fluctuations and Critical Slowing Down in the Pseudogap Phase of* $YBa_2Cu_3O_y$, Sci. Adv. **4**, eaao5235 (2018).

[61] R. Okazaki, T. Shibauchi, H. J. Shi, Y. Haga, T. D. Matsuda, E. Yamamoto, Y. Onuki, H. Ikeda, and Y. Matsuda, *Rotational Symmetry Breaking in the Hidden-Order Phase of* URu_2Si_2, Science **331**, 439 (2011).

[62] S. Kasahara, H. J. Shi, K. Hashimoto, S. Tonegawa, Y. Mizukami, T. Shibauchi, K. Sugimoto, T. Fukuda, T. Terashima, A. H. Nevidomskyy, and Y. Matsuda, *Ectronic Nematicity above the Structural and Superconducting Transition in* $BaFe_2(As_{1-x}P_x)_2$, Nature (London) **486**, 382 (2012).

[63] Y. Sato, S. Kasahara, H. Murayama, Y. Kasahara, E.-G. Moon, T. Nishizaki, T. Loew, J. Porras, B. Keimer, T. Shibauchi, and Y. Matsuda, *Thermodynamic Evidence for a Nematic Phase Transition at the Onset of the Pseudogap in* $YBa_2Cu_3O_y$, Nat. Phys. **13**, 1074 (2017).

[64] H. Murayama, Y. Sato, R. Kurihara, S. Kasahara, Y. Mizukami, Y. Kasahara, H. Uchiyama, A. Yamamoto, E. G. Moon, J. Cai, J. Freyermuth, M. Greven, T. Shibauchi, and Y. Matsuda, *Diagonal Nematicity in the Pseudogap Phase of* $HgBa_2CuO_{4+\delta}$, Nat. Commun. **10**, 3282 (2019).

[65] J.-H. Chu, H.-H. Kuo, J. G. Analytis, and I. R. Fisher, *Divergent Nematic Susceptibility in an Iron Arsenide Superconductor*, Science **337**, 710 (2012).

[66] H.-H. Kuo, J.-H. Chu, J. C Palmstrom, S. A Kivelson, and I. R Fisher, *Ubiquitous Signatures of Nematic Quantum Criticality in Optimally Doped Fe-Based Superconductors*, Science **352**, 958 (2016).

[67] M. C. Shapiro, A. T. Hristov, J. C. Palmstrom, J.-H. Chu, and I. R. Fisher, *Measurement of the* B_{1g} *and* B_{2g} *Components of the Elastoresistivity Tensor for Tetragonal Materials via Transverse Resistivity Configurations*, Rev. Sci. Instrum. **87**, 063902 (2016).

[68] S. Hosoi, K. Matsuura, K. Ishida, H. Wang, Y. Mizukami, T. Watashige, S. Kasahara, Y. Matsuda, and T. Shibauchi, *Nematic Quantum Critical Point without Magnetism in* $FeSe_{1-x}S_x$ *Superconductors*, Proc. Natl. Acad. Sci. U.S.A. **113**, 8139 (2016).

[69] K. Ishida, M. Tsujii, S. Hosoi, Y. Mizukami, S. Ishida, A. Iyo, H. Eisaki, T. Wolf, K. Grube, H. v. Loehneysen, R. M. Fernandes, and T. Shibauchi, *Novel Electronic Nematicity in Heavily Hole-Doped Iron Pnictide Superconductors*, Proc. Natl. Acad. Sci. U.S.A. **117**, 6424 (2020).

[70] K. Ishida, S. Hosoi, Y. Teramoto, T. Usui, Y. Mizukami, K. Itaka, Y. Matsuda, T. Watanabe, and T. Shibauchi, *Divergent Nematic Susceptibility Near the Pseudogap Critical Point in a Cuprate Superconductor*, J. Phys. Soc. Jpn. **89**, 064707 (2020).

[71] L. Fruchter, D. Colson, and V. Brouet, *Magnetic Critical Properties and Basal-Plane Anisotropy of* Sr_2IrO_4, J. Phys. Condens. Matter **28**, 126003 (2016).

[72] M. Nauman, Y. Hong, T. Hussain, M. S. Seo, S. Y. Park, N. Lee, Y. J. Choi, W. Kang, and Y. Jo, *In-Plane Magnetic Anisotropy in Strontium Iridate* Sr_2IrO_4, Phys. Rev. B **96**, 155102 (2017).

[73] T. Shibauchi, T. Hanaguri, and Y. Matsuda, *Exotic Superconducting States in FeSe-Based Materials*, J. Phys. Soc. Jpn. **89**, 102002 (2020).

[74] N. Auvray, B. Loret, S. Benhabib, M. Cazayous, R. D. Zhong, J. Schneeloch, G. D. Gu, A. Forget, D. Colson, I. Paul, A. Sacuto, and Y. Gallais, *Nematic Fluctuations in the Cuprate Superconductor* $Bi_2Sr_2CaCu_2O_{8+\delta}$, Nat. Commun. **10**, 5209 (2019).

[75] V. M. Yakovenko, *Tilted Loop Currents in Cuprate Superconductors*, Physica B (Amsterdam) **460**, 159 (2015).

[76] Y. Tang, L. Mangin-Thro, A. Wildes, M. K. Chan, C. J. Dorow, J. Jeong, Y. Sidis, M. Greven, and P. Bourges, *Orientation of the Intra-Unit-Cell Magnetic Moment in the High-*T_c *Superconductor* $HgBa_2CuO_{4+\delta}$, Phys. Rev. B **98**, 214418 (2018).

[77] J. Porras, J. Bertinshaw, H. Liu, G. Khaliullin, N. H. Sung, J.-W. Kim, S. Francoual, P. Steffens, G. Deng, M. M. Sala, A. Efimenko, A. Said, D. Casa, X. Huang, T. Gog, J. Kim, B. Keimer, and B. J. Kim, *Pseudospin-Lattice Coupling in the Spin-Orbit Mott Insulator* Sr_2IrO_4, Phys. Rev. B **99**, 085125 (2019).